Journal of Materials Processing Tech. 317 (2023) 117972

Contents lists available at ScienceDirect

Journal of Materials Processing Tech.

journal homepage: www.elsevier.com/locate/jmatprotec

A penetration depth monitoring method for Al-Cu laser lap welding based on spectral signals

Shixuan Li, Ping Jiang, Yu Gao, Minjie Song, Leshi Shu [*,1]

The State Key Laboratory of Digital Manufacturing Equipment and Technology, School of Mechanical Science and Engineering, Huazhong University of Science & Technology, Wuhan, Hubei 430074, China

ARTICLE INFO

Associate Editor: Fenggui Lu

Keywords:
Laser welding
Monitoring
Spectrometer
Penetration depth
Dissimilar metal

ABSTRACT

Al-Cu laser lap welding is widely applied in modern manufacture industry (e.g., electric vehicle battery pack manufacturing). Due to the inevitable penetration fluctuation, pseudo welding defects (usually shown as lack of penetration depth) commonly exist in Al-Cu welds, severely influence the strength, electrical resistance of the welds. The quality inspection of laser welded joints is very important to ensure the reliability of welding seams. Traditional off-line monitoring methods are not likely satisfying the demand of high pace manufacturing such as EV power battery manufacturing. In this paper, a novel high accuracy Al-Cu laser lap welding penetration depth monitoring method based on spectral signal is introduced. The relationship model between the ratio of specific Al and Cu spectral intensities and the penetration depth of Al-Cu laser lap welding was established based on BPNN (Back Propagation Neural Network). The accuracy of the monitoring model was tested via a set of testing experiments and the results showed that the proposed method can precisely predict the penetration depth of Al-Cu laser lap welding.

1. Introduction

Al-Cu lap welding is widely used in electric vehicle (EV) manufacturing (Dimatteo et al., 2019). For example, in EV power battery pack, aluminum and copper are commonly used as the material of the battery tab and busbar (Fig. 1) attribute to their high electrical conductivity (Sadeghian and Iqbal, 2022). Nowadays, the lap welding method includes: resistance spot welding, ultrasonic welding, arc welding and laser welding etc. (Stavridis et al., 2017). Laser welding has been widely used during the manufacturing process of EV (Das et al., 2018) due to the advantage of incomparable welding efficiency (Chelladurai Asirvatham et al., 2022), small heat affection zone, high depth-width ratio and minimal distorting (Song et al., 2021).

Reliability of the Al-Cu laser lap welding joints are the basic guarantee of high yield EV power battery manufacturing (Kuryntsev, 2021). However, laser welding is a highly dynamic process, the fluctuation of the penetration depth is inevitable due to the rapid change of key hole and weld pool. At the same time, the differences in fusion point and thermal conductivity of Al and Cu (Table 1) make it difficult to obtain a fine welding joint (Naeem and Montello, 2022). In the "wave trough" zone, weak joints of Al and Cu are likely to become pseudo welding defect and brought danger to EV use (Wang et al., 2020; Wu et al., 2021). Welds quality monitoring is essential when it refers to ensuring the reliability of the power battery of EVs. Traditional destructive monitoring methods are not able to fulfill the demand of high pace EV components manufacturing.

The forming monitoring methods based on signals that acquirable during the process of laser welding were studied and gradually utilized in the practical production. Two sorts of the widely used monitoring methods are based on visual or acoustic signals, which consist of the information of the area and the size of the weld pool, keyhole and plasma plume, and the pitch of the sound during the laser welding process. Visual and acoustic signals can be easily acquired by equipment that equipped with CCD, CMOS or microphones. Early in 1997, Beersiek et al. (1997) proposed a laser welding process monitoring method based on visual signals captured by CCD-camera and the capillary was monitored with an accuracy of ± 10%. Years later, Zhang et al. (2020) introduced an innovative convolutional neural network (CNN) based monitoring method that consist of a visual monitoring system and a penetration state analytic system. The penetration state (Partial penetration, moderate penetration, full penetration, excessive penetration) classification accuracy of the CNN model reached 94.6%. Cai et al.

* Corresponding author.
E-mail address: leshishu@hust.edu.cn (L. Shu).
[1] ORCID: 0000–0001-9168–1347

https://doi.org/10.1016/j.jmatprotec.2023.117972
Received 13 February 2023; Received in revised form 29 March 2023; Accepted 4 April 2023
Available online 6 April 2023

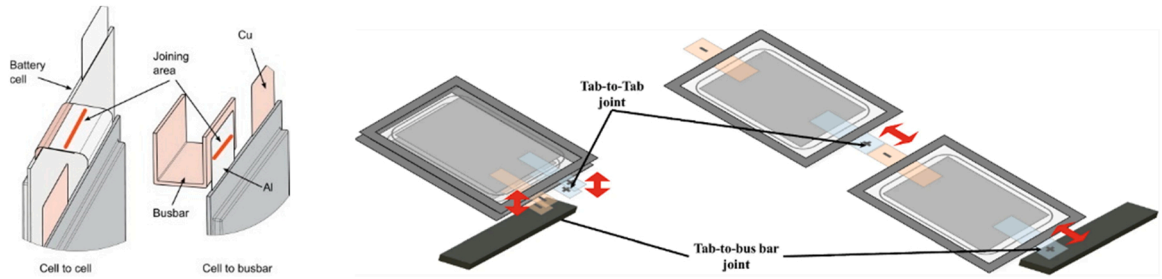

Fig. 1. The practical application of Al/Cu in e-mobility cell pack (Das et al., 2019; Solchenbach et al., 2014).

Table 1
Electrical and mechanical properties of Al and Cu and their volumetric weight and cost (Kumar et al., 2021).

Materials	Electrical properties	Mechanical properties	Volumetric weight (kg/m^3)	Cost (US $/ton)
Al	$\rho = 2.8 \times 10^{-8}$ Ω·m	TS = 90 MPa, YS = 75 MPa, SS = 70 MPa, λ = 229 W/m·K, MT = 645 ℃, $\alpha = 24 \times 10^{-6}$ ℃$^{-1}$	2700	2490.0
Cu	$\rho = 1.7 \times 10^{-8}$ Ω·m	TS = 210 MPa, λ = 391.1 W/m·K, MT = 1083 ℃, $\alpha = 16 \times 10^{-6}$ ℃$^{-1}$	8960	10,029.0

Note: ρ = Electric resistivity, TS = Tensile strength, YS = Yield strength, SS = Shear strength, λ = Thermal conductivity, MT = Melting temperature, α = Coefficient of thermal expansion.

(2022) proposed a novel penetration classification method based on deep neural networks methods and proved that the monitoring method could reach 98.68% prediction accuracy. Early in 1995, Gu and Duley (1995) studied the acoustic emission during the process when laser beam interacted with the materials, they found that the harmonic components shows different characteristic when the penetration status are different. Yusof et al. (2017) acquired sound signals during the laser welding process. The sound dynamics in time domain, frequency domain was analyzed prior to the support vector machine classification analysis. They concluded that the features that extracted via synchrosqueezed-wavelet analysis were useful in classifying sound signals from different penetration status. Comparing to the half/full penetration classification with BP, the Cumulative Sychrosqueezed-wavelet classification method improved the accuracy from 91.94% to 96.94%(Yusof et al., 2020). Based on the researches of the laser welding monitoring methods introduced above, some researches proposed some monitoring methods based on multiple signals (Nilsen et al., 2017; Oezmert et al., 2013). Based on the images captured by high speed camera, Zhang et al. (2018) found that the variation of the centroid height plasma plume and keyhole constantly located in low-frequency component (0–400 Hz). With the help of BPNN, Li et al. (2022) analyzed the relationship between the images and spectrum of plasma plume and penetration depth, they found that the area and centroid height of plasma are highly related to the penetration states. The BPNN model based on plasma plume-based multi feature was able to predict the penetration state with an accuracy of 97%. Zhang et al. (2019) used a monitoring system that employed a multi-band visual system, a spectrometer and a photodiode to capture signals of the laser welding process. A monitoring system based on a deep belief network was then established and was proved to be high-precision and high robustness in welding status monitoring (sound well weld, blowout, humping, undercutting). However, the weld penetration status (non-sufficient penetrated welds, full penetrated welds, over penetrated

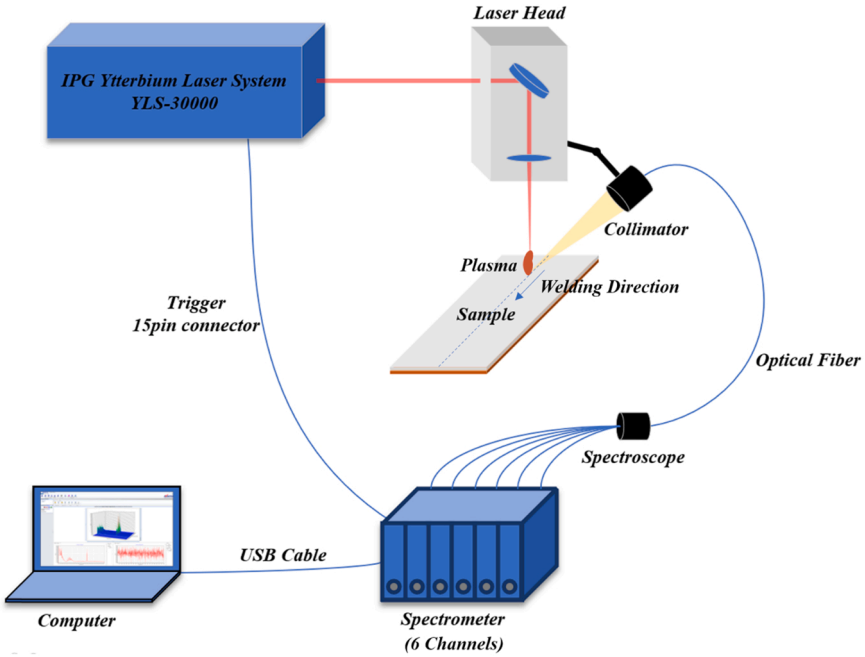

Fig. 2. Laser welding experimental system with optical spectrum acquisition.

Table 2
Chemical Composition Value in Samples (wt%).

Element				Al	Si	Fe	Cu	Mn	Mg	Cr	Zn	Ti	
Actual Chemical Composition Value				99.65	0.08	0.16	0.03	0.02	0.01	0.16	0.01	0.01	
Element	Cu+Ag	P	Bi	Sb	As	Fe	Ni	Pb	Sn	S	Zn		O
Actual Chemical Composition Value	99.9929	0.0012	0.0003	0.0001	0.0002	0.001	0.0006	0.001	0.0002	0.0005	0.0004		0.001

welds) classification model established in these studies are not likely quantitatively monitoring the penetration depth.

In recent years, spectral signal based laser welding penetration monitoring methods have been received plenty of concentration (Chen et al., 2013; Lehmann et al., 2013). Yu et al. (2020) presented a quality monitoring method based on deep neural network in laser welding process, reached nearly 90% penetration classification (unwelded, incomplete penetration, full penetration, unwelded by a gap) accuracy. Sibillano et al. (2010) proposed several studies based on the spectroscopic analysis of the plasma plume collected during the laser welding process. The electron temperature of plasma plume was estimated. They found that the electron temperature had a clear trend of decreasing when the welding laser power increased (Sibillano et al., 2012a). They maintain that this counterintuitive pattern of change may have something to do with the fact that at deeper penetration, the hottest core of the plume moves down into the evaporative capillary, so that the plasma temperature measured at the top of the pore appears to be lower at higher incident power. Such a quantitative relationship between the electron temperature signal and the penetration depth was used as the indicator of a laser power feed-back control system which was proved valid in penetration depth closed-loop control (Sibillano et al., 2012b). Oppositely, Chen et al. (2019) organized their galvanized steel laser welding experiments and found that the electron temperature had a clear trend of increasing when the welding laser power increased, the temperature and spectral intensity of the plasma plume varies when the welded samples have different sheet gaps. The relation between the plasma plume electron temperature and penetration depth still remains uncertainty. Plenty of works have proved that plasma spectra are able to reflect the particle concentration in the laser-sample interaction zone (Guo et al., 2013; Lednev et al., 2021; Yang et al., 1995). Schmalen et al. (2018) found that when the laser interacts with different materials (Al and Cu), the increase of Al/Cu-specific peak in the emission spectra could be detected. Based on existed studies, the differences lie among spectral intensities could provide data support to the penetration depth monitoring model in dissimilar metal laser lap welding. However, the study in this area still remains blank.

In this paper, a novel Al-Cu laser lap welding penetration depth monitoring method based on the spectral signal of plasma plume is introduced. The spectral information of several Al and Cu lines under different laser power were extracted. The quantitative Al-Cu laser lap welding penetration depth monitoring model based on the ratio of Al and Cu spectra intensities was established based on BPNN. The accuracy of the method was tested via a set of testing experiments.

2. Experimental

The schematic diagram of the experimental device is shown in Fig. 2.

A multi-mode IPG YLS-30000 Ytterbium laser system was used in the experiment. The working wavelength was 1070 nm and the maximum output laser power was 30 kW in continuous wave state. The laser beam was focused on the sample through a parabolic focusing mirror with a focal length of 74 mm. The laser head was attached to the end of a fully automatic 6-axis KUKA robot unit. A 3 mm thick Al1060 plate was superimposed on a 2 mm thick TU1 Cu plate, the lap welding experiment was carried out and the length of weld seams were kept at 100 mm. The welding speed was maintained at 35 mm /s and the defocusing distance from the sample surface was maintained at − 3 mm. The argon protection flow rate is 15 L/min and the nozzle distance is 6 mm. Through experiments, the laser power is set in the range of 4.8 kW ~ 6 kW with 200 W gap to obtain different penetration depth. The plasma optical emission has been collected by a 6 mm focal length collimator placed at a 45° Angle to the laser beam axis, 200 mm from the focus. The collected plasma light signal was sent through a 200-um core fiber to the spectrometer, which divides the signal into eight parts, six of which were transmitted to the fast spectrometer, and the remaining two were used for calibration and backup. The model of the fast spectrometer was AvaSpec-UL32048Cl-6-EVO. The spectrometer employs six channels with different spectral bandwidth, respectively, spectral bandwidths of six channels are 200–363 nm, 362–512 nm, 511–611 nm, 610–705 nm, 704–887 nm and 886–1100 nm. The optical signals with different spectral bandwidths were collected by channels whose serial number varies from 2111155U6 to 2111156U6 and mean optical resolution varies from 0.1 nm to 0.28 nm. Table 2.

In this research, 35 pairs of samples were welded with laser power varies from 4.8 kW to 6 kW, the data obtained in 28 experiments were used as the training set of the BPNN and the rest 7 experiments (one for each different laser power) were used to verify the prediction accuracy. To obtain the accurate penetration depth of each weld seam, joints were cut transversely every 10 mm, 18 cross sections of each weld seam were analyzed and the mean value of penetration depth extraction result of all the sections were regarded as the penetration depth of the weld seam.

3. Theoretical background

3.1. Theoretical background

The spectral intensity/counts stand for the electromagnetic radiation intensity. The counts shown on the interface of Avasoft software (the spectrometer data processing software) represent the voltage data produced by CMOS in the spectrometer during the interaction between CMOS pixels and electromagnetic radiation, the higher electromagnetic radiation intensity, the higher voltage produced by CMOS. Therefore, the fluctuation of electromagnetic radiation intensity is detected by the spectrometer. According to Boltzmann Equation, based on the assumptions that the laser- induced plasma is optically thin and in local thermal equilibrium, the laser-induced plasma emitted electromagnetic radiation intensity could be calculated the followed way (Chen et al., 2013):

$$I = n_s A_{ij} g_i h v_{ij} \bullet \exp(-E_i/kT)/Z \quad (1)$$

in which I is spectral intensity, respectively, E_i and g_i are the energy and the degeneracy of the upper energy level, A_{ij} is the transition probability, Z is the partition function, k is the Boltzmann constant, T is the electron temperature, n_s is the particle concentration in the laser-induced plasma, h is the Planck constant, v is the frequency of the radiation. Let f be the function of Z and T, $A_{ij}g_i v_{ij}\exp(-E_i/kT)/Z$. Then, the particle concentration ratio of different particles in the laser-induced plasma can be calculated and simplified the followed way:

$$n_{s1}/n_{s2} = A_{ij1} g_{i1} Z_2 v_{ij1} \exp((E_{i2} - E_{i1})/kT) I_1 / A_{ij2} g_{i2} v_{ij2} Z_1 I_2 = f_1 I_1 / f_2 I_2 \quad (2)$$

in which the subscribe character 1 and 2 represent two different particles exist in the laser-induced plasma. On the basis on this equation, the particle concentration ratio could be regarded as a first order nonlinear function of the ratio of corresponding spectral intensities, which means that the relativity between these two ratios is strong.

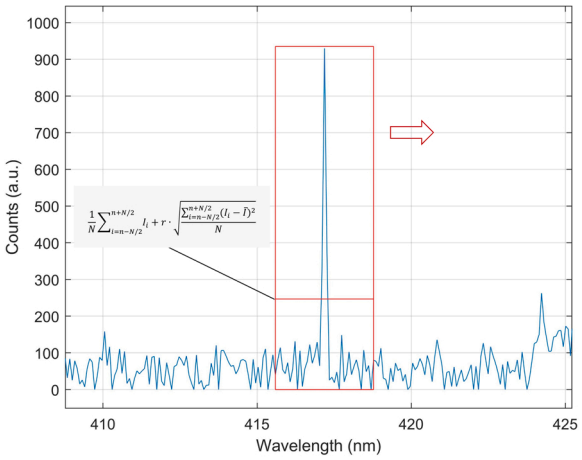

Fig. 3. Spectral analyze based on sliding window method.

3.2. Extraction of continuous characteristic spectral lines

The spectral data got from the fast spectrometer contains the intensity information of thousands of spectral lines whose wavelengths lies between 200 nm and 1100 nm. However, only a few of them were distinguishable spectral lines (characteristic spectrum lines), even less were continuously detected throughout the laser welding process. The first thing of spectral data analysis is to find continuous distinguishable spectral lines throughout the process of laser welding.

As shown in Fig. 3, a sliding window of size N was set to extract the distinguishable spectral lines that satisfies the equation:

$$I_n > \sum_{i=n-N/2}^{n+N/2} I_i \Big/ N + r \bullet \sqrt{\sum_{i=n-N/2}^{n+N/2} (I_i - \bar{I})^2 \Big/ N} \tag{3}$$

in which I means the spectral intensity, respectively, n stands for the number of the analyzed spectral line, N stands for the size of the sliding window and r is the comparison coefficient. The coefficient that in-

Table 3
Information of important spectral lines (Kramida, 2022).

	Ritz Wavelength (nm)	A_{ji} (s^{-1})	E_i (cm^{-1})	E_j (cm^{-1})	Lower Level Conf., Term, J	Upper Level Conf., Term, J
Al I	308.2151	5.87e+ 07	0	32,435.453	$3s^2 3p\ 2P^\circ\ 1/2$	$3s^2 3d\ 2D\ 3/2$
	309.27084	7.29e+ 07	112.061	32,436.796	$3s^2 3p\ 2P^\circ\ 3/2$	$3s^2 3d\ 2D\ 5/2$
	394.40060	4.99e+ 07	0	2537.756	$3s^2 3p\ 2P^\circ\ 1/2$	$3s^2 4s\ 2S\ 1/2$
	396.15201	9.85e+ 07	112.061	25,347.756	$3s^2 3p\ 2P^\circ\ 3/2$	$3s^2 4s\ 2S\ 1/2$
Cu I	324.75358	1.395e+ 08	0	30,783.697	$3d^{10} 4s\ 2S\ 1/2$	$3d^{10} 4p\ 2P^\circ\ 3/2$
	327.39521	1.376e+ 08	0	30,535.324	$3d^{10} 4s\ 2S\ 1/2$	$3d^{10} 4p\ 2P^\circ\ 1/2$
	578.2126	1.65e+ 06	13,245.443	30,535.324	$3d^9 4s^2\ 2D\ 3/2$	$3d^{10} 4p\ 2P^\circ\ 1/2$

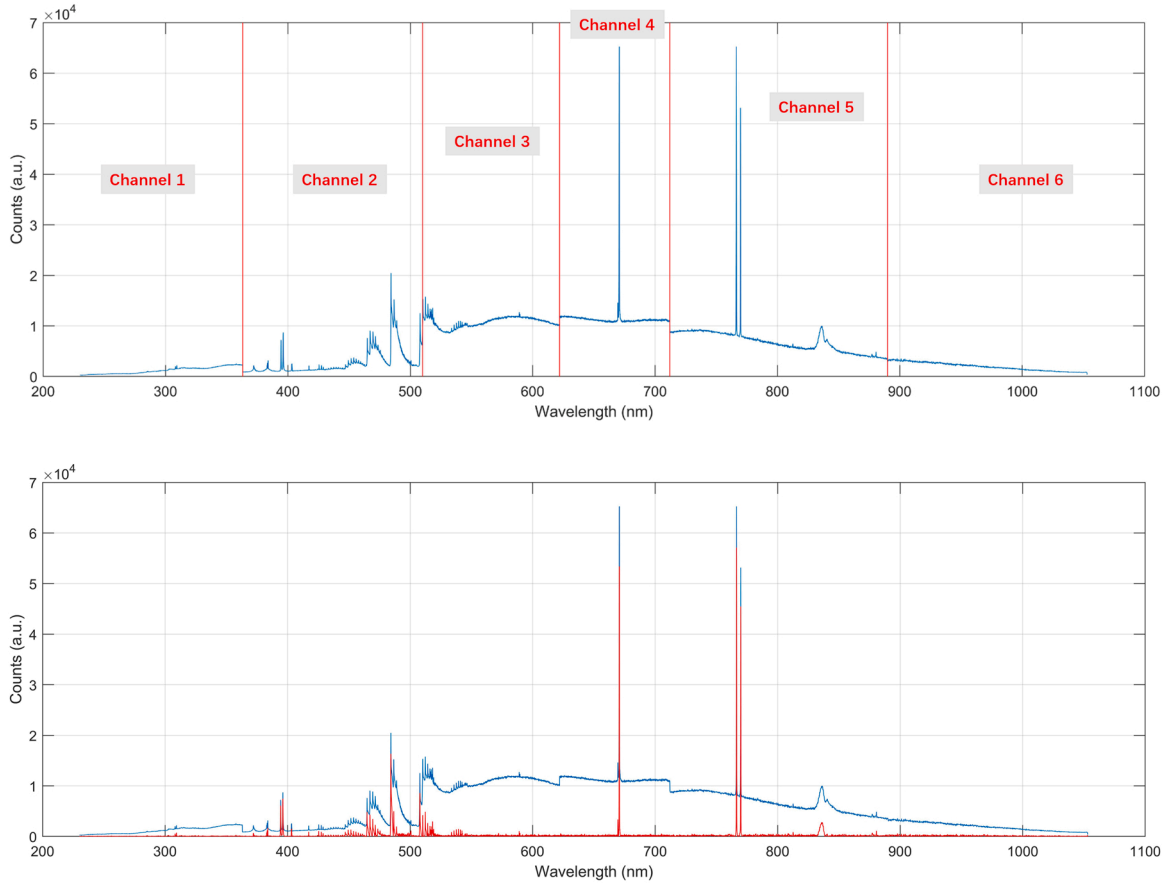

Fig. 4. Multichannel separation of the line spectrum from the background.

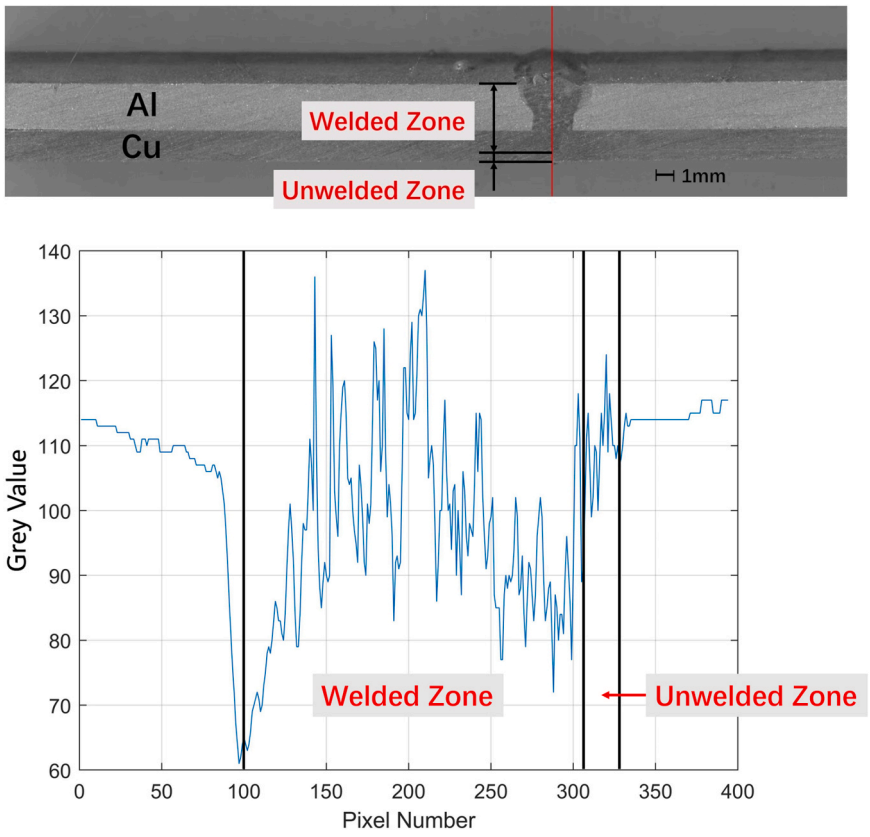

Fig. 5. The grey value of the image at deepest weld crosssection.

fluences the extraction result most is *r*. A larger number of lines could be extracted if a relatively small value of *r* is chosen, which could cause a heavy work when analysis the extracted lines. On the other side, if a relatively large value of *r* is chosen, the number of the extracted lines could be less than existed characteristic spectrum lines, which could lead to information loss. After several times of experiments, 1.3 is found to be the proper value of *r* that could extract the characteristic spectrum efficiently. The value of *N*, which means the number of detected spectra in the sliding window, should be set slightly smaller than twice the smallest gap between two distinguishable lines that corresponding to adiation with different lower energy level. In this research, the value of *N* was set to 40.

The result of distinguishable spectral line extraction shows that characteristic spectral lines with 62,055 different wavelengths were extracted out of 10,636 different wavelengths of spectra data, most of them just appeared a few times, 685 of them even appeared just once in the whole process of laser welding. Considering of approximately 8.35 ms each frame might take (including integration time and data processing and transmission time) and about 3.4 s of welding time, there are approximately 400 frames that contains the information of laser-induced plasma radiation. To ensure that the chosen characteristic lines can be used for laser welding process in-situ monitoring, 61 spectral lines that appeared in more than 80 frames were extracted out of 10636 spectral data at last as continuous characteristic spectral lines. After comparing the wavelengths of these 61 spectral lines with the database of NIST (Kramida, 2022), 7 of them are Cu or Al lines (Table 3), 53 of them are derived from the radiation of the plasma of elements from welding samples.

3.3. Separation of line spectrum based on multi-channel second lower enveloping method

After the process above, characteristic spectral lines that continuously exist throughout the whole laser welding process were extracted. As is shown in Fig. 4, the intensity of them, however, is determined by not only the corresponding ionized element's emitted radiation but also the spatial error between different channels and the background spectral intensity (including AlO radical etc.) (Guo et al., 2013). For further calculation, the needed ionizing radiation intensity has to be separated from the background spectrum and the spatial error has to be eliminated.

To eliminate the spatial error, the background spectrum is separated in different channels of each frame. Not like needlelike ionized metal atom spectral lines, the background radiation spectrum is smoother in wavelength dimension, which makes the method of second lower enveloping useful in the process of line spectrum separation. Firstly, every local minimum point was found, then cubic spline method was used to fit the background spectrum. Repeating this process for another time, then the background spectrum could be separated, which also means that needle-like spectrum is separated from the original spectrum (Fig. 4).

3.4. Penetration depth extraction

Considering the fact that the bottom of the penetrated zone is just about 1 mm width. Whereas, when cutting the welds lengthways, it is hard to keep the cross section through the bottom of the weld. To eliminate the penetration depth extraction error contributed by welds cutting process, the welds were cut into ten pieces crosswise, the cross sections were polished, scanned, the scan image of each section were analyzed and the mean penetration depth value of all the crosswise pieces in a single weld was regard as the practical penetration depth.

Turning the picture into grey image and find a threshold to obtain the desired outline is a commonly used method in the field of picture processing. In this case, however, the difference between welded zone and base metal zone in the grey image is hard to tell (Fig. 5). Consider of the

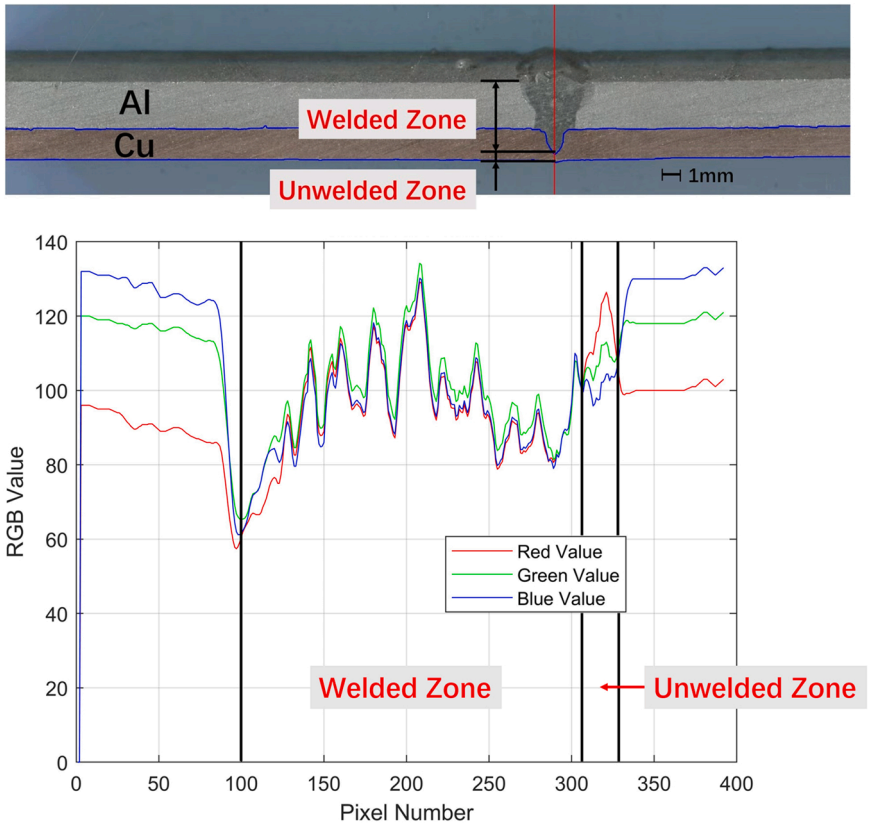

Fig. 6. The RGB value of the image at deepest weld crosssection.

significant color difference between two zones, a RGB color analysis method is used to obtain penetration depth in this research.

As is shown in Fig. 6, is the figure of RGB value of the cross-section image, in the lower base metal region, the red value is relatively higher than the value of green and blue signal. Therefore, the RGB value and the proportion of red and green/blue value can be used to obtain the number of the pixels that represent lower base metal in the weld scan image (the region between the blue lines). The average number of pixels in the vertical direction of the unwelded area of the lower plate is 63. For the reason that the thickness of the lower base metal is 2 mm, the length that each pixel represent in vertical direction is about 0.033 mm. Multiply the number of pixels by the length of each pixel, we can find the thickness that is not penetrated (Unwelded Zone in Fig. 6). The penetration depth is then obtained by subtracting the unpenetrated thickness from the total plate thickness.

4. Proposed method

4.1. The analysis of the relation between spectral intensity ratios and penetration depth

The spectrometer's working time is in sync with the shielding gas.

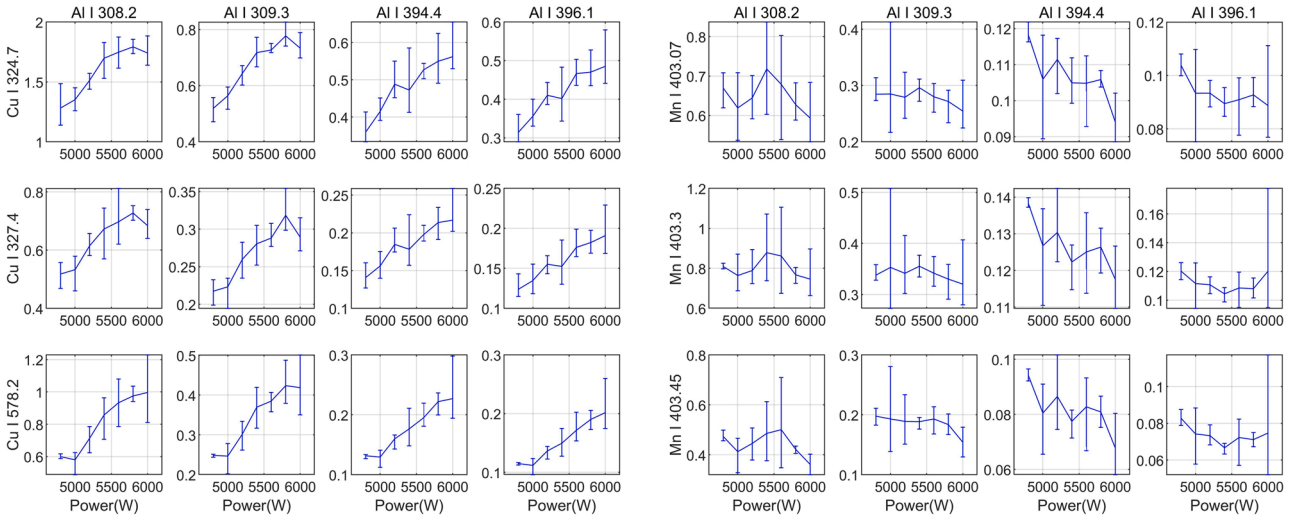

Fig. 7. Spectral intensity ratios of (a) Cu I/Al I and (b) Mn I/Al I lines.

The time range of acquiring laser-induced plasma spectra data, therefore, is a bit longer than the actual time range of the laser welding process. To obtain spectral information just right during the welding process, Na I line with a wavelength of 588.99 nm (captured via channel three), which is constantly distinct in spectra, is used to segment the obtained spectra in time range.

As mentioned above, Cu I lines with wavelengths of 324.7 nm, 327.4 nm (captured via channel two) and 578.2 nm (captured via channel three) and Al I lines with wavelengths of 308.2 nm, 309.3 nm (captured via channel one), 394.4 nm and 396.1 nm (captured via channel three) were used to calculate the spectral intensity ratio of Cu I and Al I spectral lines in the whole process of laser welding. To eliminate the possible integral spectral influence to the result, the Mn I lines with wavelengths of 403.07 nm, 403.3 nm and 403.45 nm (captured via channel two) were used to calculate the spectral intensity ratio of Mn I lines and Al I lines as the comparison group. The mean spectral intensity value of all the lines mentioned above in thirty-five welds were calculated to obtain the spectral intensity ratio. These thirty-five welds were consisted of seven sets of welds with different welding power varies from 4800 W to 6000 W, each set of welds has five welds that welded with the same welding parameter. The variation tendency of spectral intensity ratio in these five sets of experiments are shown in Fig. 7.

Fig. 7(a) shows the variation tendency of the Cu/Al spectral intensity ratio and Fig. 7(b) shows the variation tendency of Mn/Al spectral intensity ratio. As the laser power increases, the Cu/Al spectral intensity ratio has an obvious increasing tendency, as for the Mn/Al spectral intensity ratio (the comparison group), the tendency is much more disordered, which means that the increasing tendency is not a general feature of spectral intensity ratios other than Cu and Al characteristic spectral lines in these sets of experiments. In the other words, the increasing tendency of Cu/Al spectral intensity ratio is possibly due to a kind of change directly proportional to the change of laser power, that relevant to the source of Cu I and Al I spectral lines only. The source of Mn I lines, however, is the same as the source of Al I lines, which makes the ratio of the spectral intensity of them are not quite relevant with the change of the laser power.

Another feature of the distribution of Cu/Al spectral intensity ratio is that the increasing tendency of them is more obvious and smoother in the last row of subplots in Fig. 7(a), which are the ratio of Cu I spectral line with a wavelength of 578.2 nm that lies in the channel three and Al I lines. The difference between the last row of ratios and previous ones is that the spectral lines used to calculate the ratio in the last row have the biggest wavelength difference. This phenomenon is caused by the fact that the fluctuation of the spectral lines that lies near each other is tend to have a similar change pattern. This similar change pattern can also be found between the first row and the second row, the first column and the second column, the third column and the last column. These sets of subplots represent the ratio that result from either nearby Cu lines (324.7 nm, 327.4 nm) or nearby Al lines (308.2 nm, 309.3 nm and 394.4 nm, 396.1 nm). Inevitably, the spectral intensity ratio fluctuation caused by the variation of particle concentration is easy to be coupled with the similar changing pattern of nearby spectral lines. This feature leads to a result that the ratio between two spectral intensities with larger wavelength difference is tend to have a better particle concentration ratio representation capacity. Comparing to single channel spectra monitoring methods, multi-channel methods have an irreplaceable advantage of larger wavelength range.

According to the theoretical background demonstrated above, the increasing tendency of Cu/Al spectral intensity ratio may due to the change of penetration depth brought by the change of the laser power in different sets of experiments. The spectral intensity ratio has a strong correlation with the corresponding particle concentration in laser-induced plasma. Furthermore, the particle concentration, particularly the particle source from different material in the case of dissimilar metal lap joint laser welding, is determined by the penetration depth. As long as the upper sample is fully penetrated, the particle concentration of Al or other elements that only exist in the upper sample is supposed to be relatively constant. The particle concentration of Cu or other element that exist in the lower plate, however, is supposed to be varied in different set of experiments for the reason that different laser power result in different penetration depth. Consequently, the change of penetration depth result in the ratio variation of the spectral intensity that source from these elements. To obtain a more specific relation between spectral intensity ratios and penetration depth, the next step is to obtain the penetration depth in different set of experiments.

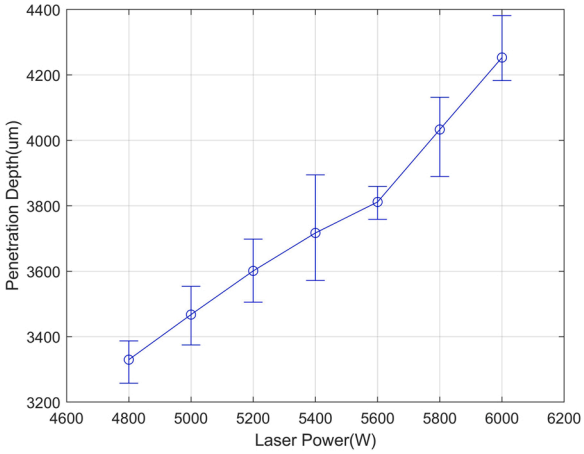

Fig. 8. Penetration depth variation.

In the experimental set with a laser power of 6 kW, full penetration and over penetration part exist in the welds. Considering of the fact that over penetration only happened in few points in this set of experiments, the penetration depth was calculated as 5 mm (fully penetration depth) with little loss of accuracy to integral penetration depth. As the laser power increases from 4.8 kW to 6 kW, the penetration depth varies from 3.3 mm to 4.2 mm, the standard deviation varied from 34.18 μm to 133.17 μm and kept an increasing tendency except the fourth set of experiment. The deviation percentage varies from 1.02% to 3.58%, the mean deviation is 84.85 μm, the biggest absolute deviation value happened when the laser power is 5.4 kW. It comes to a conclusion that the experience-based penetration depth prediction is not precise enough for practical use. Though the deviation of each set of experiment increases when the laser power increase, the depth value cross section was kept less than one seventh the penetration depth distribution range of different sets of experiments. The mean value of the penetration depth increases smoothly from 3.3 mm to 4.2 mm as the laser power increases from 4.8 kW to 6 kW. Though the absolute difference between the range of penetration depth and the spectral intensity ratio is huge, the variation tendency of mean penetration depth in Fig. 8 is marvelously similar to the variation tendency in the last two spectral intensity ratio subplots in Fig. 7 (Spectral intensity ratio of Cu I 578.2 nm line and Al I 394.4 nm, 396.1 nm lines). Once again, the spectral lines with larger wavelength difference wins when it comes to the correlation between spectral intensity ratio and penetration depth.

4.2. Al-Cu laser lap welding penetration monitoring model

As demonstrated before, theoretical speaking, the particle concentration can be expressed as a function of the corresponding spectral intensity. The penetration depth, therefore, can be regarded as a function of the spectral intensity ratio and the relation between them is supposed to be nonlinear (impossible to find a constant coefficient). Nonetheless, under fitted circumstance, the function between the spectral intensity ratio and the penetration depth is ought to be fixed. Based on the spectral intensity ratio and the penetration depth acquired above, the changing pattern of the correlation of them with the change of laser power is then obtainable. As shown in the Fig. 9, the red circles are

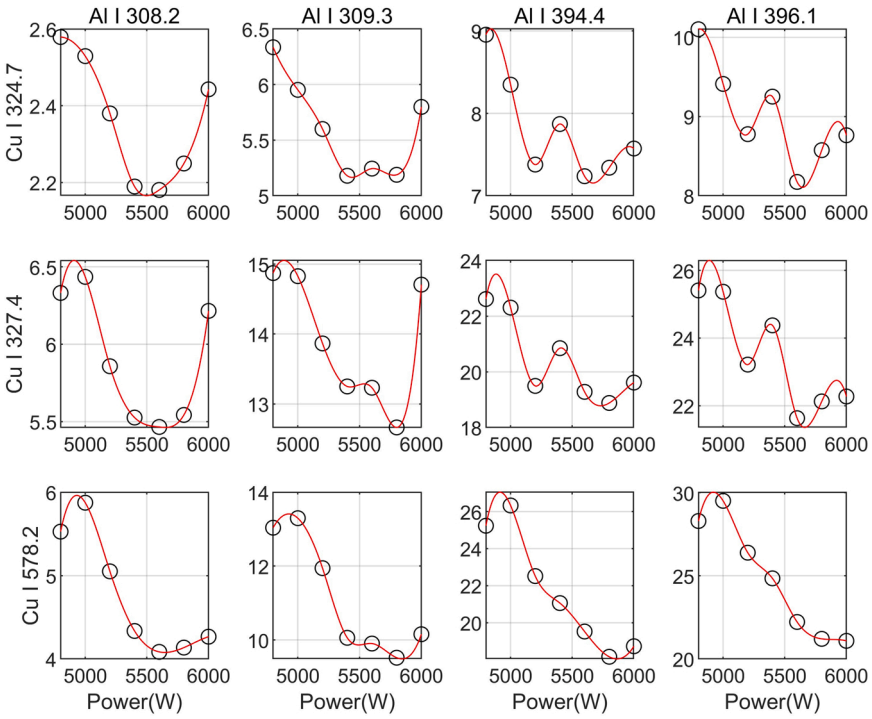

Fig. 9. Correlation between penetration depth and spectral intensity ratios.

statistical analysis data of the correlation between the spectral intensity ratio and the penetration depth and the redlines are the fitting result using the method of cubic spline interpolation. The cubic spline interpolation is defined as followed functions:

$$S(x) = \sum_{i=1}^{n-1} S_i(x), x \in [x_i, x_{i+1}] \tag{4}$$

$$S_i(x) = a_i(x - x_i)^3 + b_i(x - x_i)^2 + c_i(x - x_i) + d_i, x \in [x_i, x_{i+1}] \tag{5}$$

in which, $S_i(x)$ is the cubic polynomial function, $S(x)$ is the point participating in interpolation operation, n is the number of points participating in interpolation. The function value, first derivative and second derivative of the cubic polynomial function are continuous at the endpoints, and the function value at the interpolation point is equal to its actual value. So,

$$a_i{h_i}^3 + b_i{h_i}^2 + c_i h_i + d_i = d_{i+1} \tag{6}$$

$$3a_i{h_i}^2 + 2b_i h_i + c_i = c_{i+1} \tag{7}$$

$$6a_i h_i + 2b_i = 2b_{i+1} \tag{8}$$

in which, $h_i = x_{i+1} - x_i$ is the distance between two adjacent interpolation points. Then set the first derivative values of $S(x)$ at x_l and x_r equal to k_1 and k_2 respectively to solve the coefficients a_i, b_i, c_i and d_i of all polynomial functions.

Considering the fact that the sensitivity of different spectral lines ratio to particle concentration varies. The relationship between the predicted penetration depths based on different spectral intensity ratios and the actual penetration depth was determined using a BPNN model which has three hidden layers, the structure and hyperparameter settings of the BPNN model are shown in Fig. 10.

4.3. Model accuracy verification

To verify the accuracy of this method, a set of experiments were used as the test group. The laser power used in this set of test group varies from 4.8 kW to 6 kW, respectively, the welding speed was kept constantly at 35 mm/s, the defocusing distance was − 3 mm, the flow

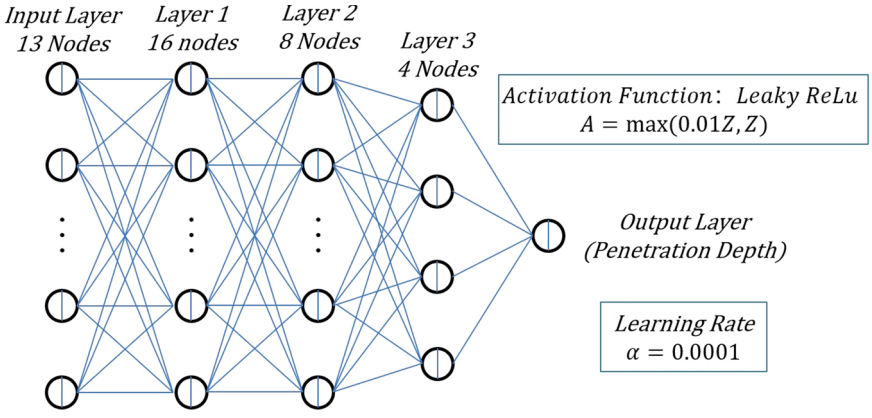

Fig. 10. The structure and hyperparameter settings of the BPNN model (Dai and MacBeth, 1997).

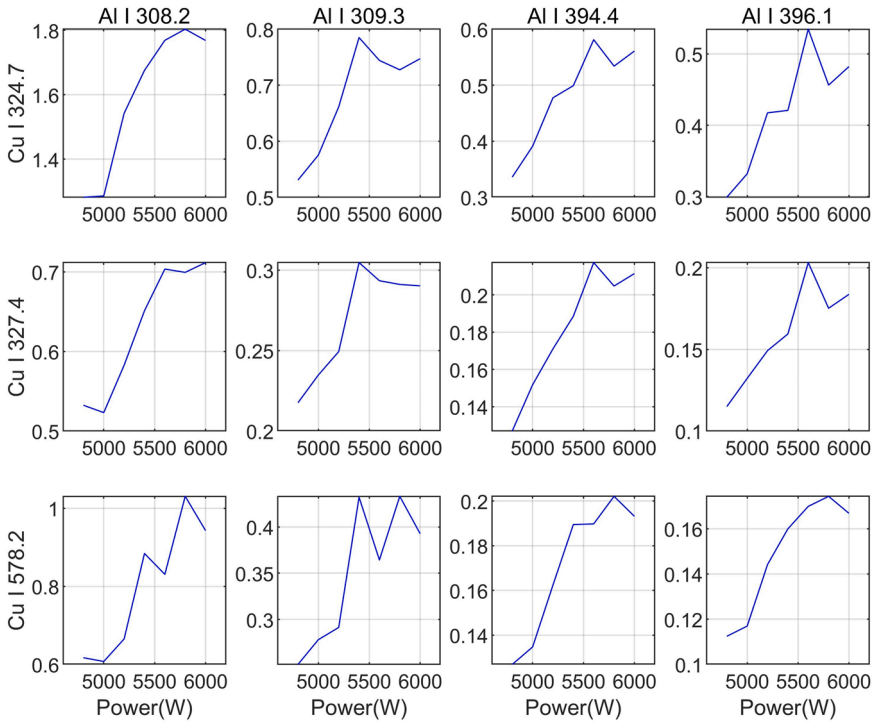

Fig. 11. The spectral intensity ratio of the test set.

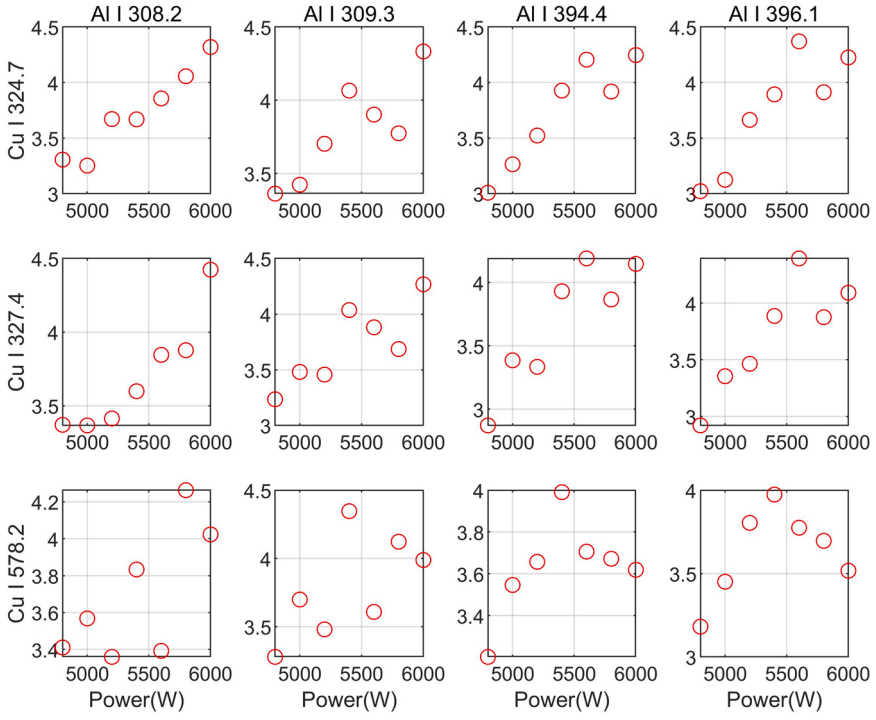

Fig. 12. The predicted penetration depth(mm) via different ratio.

rate of shielding gas was kept 15 L/min, the distance and the angel with the respect to the laser beam, etc. was kept the same as the experiments before. The intensity ratio of the selected spectral lines of this set of testing group of experiments are shown in the Fig. 11.

Based on the correlation between penetration depth and spectral intensity ratios calculated above, and the spectral intensity ratios obtained in the testing set of experiments, the predicted penetration depth of each spectral intensity ratio are listed in the Fig. 12.

The predicted penetration depths of the welds based on different pairs of spectral lines are supposed to have similar increasing tendency when the laser power increases. However, the fact is that the increasing tendency is not clear enough to make a penetration depth increasing judgment in a few of the predictions. Therefore, a conclusion can be made that a single pair of spectral intensities cannot be regarded as the support of an accurate penetration depth prediction. Based on the result of the BPNN model obtained previously, all these twelve predictions

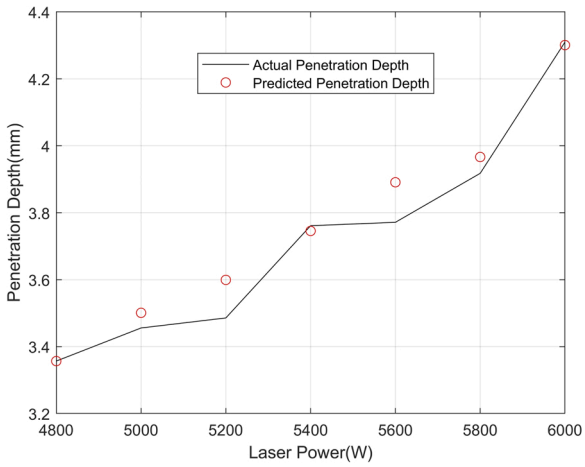

Fig. 13. The result of the penetration depth prediction.

were integrated to make an ultimate penetration depth prediction (Fig. 13) (Table 4).

Comparing to the actual penetration depth, the prediction result has a mean error of 0.05 mm, five predictions of the seven experiments have errors less than 0.1 mm. The predicted penetration depth has an almost identical tendency as the actual penetration depth.

5. Conclusions

In this paper, a novel Al-Cu laser lap welding penetration depth monitoring method based on the spectral signal of plasma plume is introduced. The main conclusions can be draw as follows.

(1) Based on the Al-Cu laser lap welding experiments, it is found that the differences in spectral intensities of specific aluminum and copper lines can reflect the variation of penetration depth, which lays the foundation of Al-Cu laser lap welding penetration depth monitoring.
(2) The ratio of the specific spectral intensities and the penetration depth have high correlation, but the approximate functional relationship between them varies under different laser power.
(3) Based on BPNN, the Al-Cu laser lap welding penetration depth monitoring model under different laser power was established. The testing result showed that the proposed penetration depth prediction method can achieve 0.05 mm monitoring accuracy.

In the future, we will integrate the proposed penetration depth monitoring method with an accuracy of 0.05 mm in the laser head and the monitoring system will play the role of defect detection and quality control in the manufacturing of power battery of e-mobility.

CRediT authorship contribution statement

Shixuan Li: Data curation, Formal analysis, Investigation, Methodology, Validation, Writing – original draft, Writing – review & editing. **Ping Jiang**: Guidance, Supervision. **Yu Gao**: Image processing, Biomimetic parameters extraction. **Minjie Song**: Assist in calculating stress intensity factors. **Leshi Shu**: Conceptualization, Project administration, Supervision, Writing – review & editing.

Table 4
The result of the penetration depth prediction.

No.	Laser Power (W)	Predicted Penetration Depth (mm)	Actual Penetration Depth (mm)	Cross Section Image
1	4800	3.36	3.36	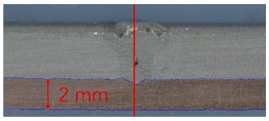
2	5000	3.50	3.46	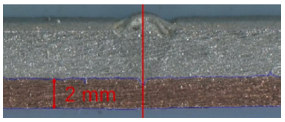
3	5200	3.60	3.49	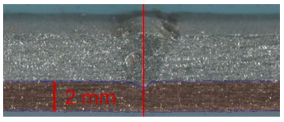
4	5400	3.75	3.76	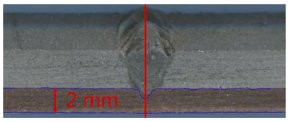
5	5600	3.90	3.77	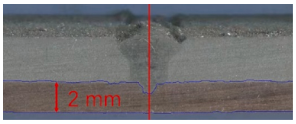
6	5800	3.97	3.92	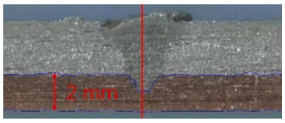
7	6000	4.30	4.31	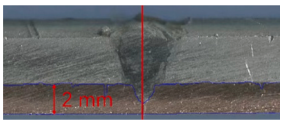

Declaration of Competing Interest

The authors declare that they have no known competing financial interests or personal relationships that could have appeared to influence the work reported in this paper.

Data availability

Data will be made available on request.

Acknowledgements

This work was supported by National Natural Science Foundation of China (NSFC), China [grant numbers 52188102, 52075201, U22A20196], National Natural Science Foundation of China National Outstanding Youth Science Fund Project, China, No. 52105256 and GuangDong Basic and Applied Basic Research Foundation, China, No.2023A1515010081. Last but not least, specially thanks to loved Min Hu for her support and contribution.

References

Beersiek, J., Poprawe, R., Schulz, W., Gu, H., Mueller, R.E., Duley, W.W., 1997. On-line monitoring of penetration depth in laser beam welding. Int. Congr. Appl. Lasers Electro-Opt. C30–C39.

Cai, W., Jiang, P., Shu, L., Geng, S., Zhou, Q., 2022. Real-time identification of molten pool and keyhole using a deep learning-based semantic segmentation approach in penetration status monitoring. J. Manuf. Process. 76, 695–707.

Chelladurai Asirvatham, M., Collins, S., Masters, I., 2022. Laser wobble welding of steel to Aluminium busbar joints for Li-ion battery packs. Opt. Laser Technol. 151.

Chen, B., Chen, Z., Cheng, H., Tan, C., Feng, J., 2019. Spectral analysis of the plasma emission during laser welding of galvanized steel with fiber laser. Trans. Intell. Weld. Manuf. 47–64.

Chen, G., Zhang, M., Zhao, Z., Zhang, Y., Li, S., 2013. Measurements of laser-induced plasma temperature field in deep penetration laser welding. Opt. Laser Technol. 45, 551–557.

Dai, H.C., MacBeth, C., 1997. Effects of learning parameters on learning procedure and performance of a BPNN. Neural Netw. 10, 1505–1521.

Das, A., Li, D., Williams, D., Greenwood, D., 2018. Joining technologies for automotive battery systems manufacturing. World Electric Vehicle J. 9.

Das, A., Li, D., Williams, D., Greenwood, D., 2019. Weldability and shear strength feasibility study for automotive electric vehicle battery tab interconnects. J. Braz. Soc. Mech. Sci. Eng. 41.

Dimatteo, V., Ascari, A., Fortunato, A., 2019. Continuous laser welding with spatial beam oscillation of dissimilar thin sheet materials (Al-Cu and Cu-Al): Process optimization and characterization. J. Manuf. Process. 44, 158–165.

Gu, H., Duley, W.W., 1995. Acoustic emission from modulated laser beam welding of materials. Int. Congr. Appl. Lasers Electro-Opt. 749–758.

Guo, L.-B., Hao, R.-F., Hao, Z.-Q., Li, K.-H., Shen, M., Ren, Z., Li, X.-Y., Zeng, X.-Y., 2013. Study on the emission spectrum of AlO radical B2+X2+ transition using laser-induced breakdown spectroscopy. Acta Phys. Sin. 62.

Kramida, A., Ralchenko, Yu., Reader, J., and NIST ASD Team (2022). NIST Atomic Spectra Database (ver. 5.10), [Online]. Available: https://physics.nist.gov/asd [2023, April 6]. National Institute of Standards and Technology, Gaithersburg, MD. DOI: https://doi.org/10.18434/T4W30F.

Kumar, N., Masters, I., Das, A., 2021. In-depth evaluation of laser-welded similar and dissimilar material tab-to-busbar electrical interconnects for electric vehicle battery pack. J. Manuf. Process. 70, 78–96.

Kuryntsev, S., 2021. A Review: Laser Welding of Dissimilar Materials (Al/Fe, Al/Ti, Al/Cu)—Methods and Techniques, Microstructure and Properties. Materials 15.

Lednev, V.N., Sdvizhenskii, P.A., Stavertiy, A.Y., Grishin, M.Y., Tretyakov, R.S., Asyutin, R.D., Pershin, S.M., 2021. Online and in situ laser-induced breakdown spectroscopy for laser welding monitoring. Spectrochim. Acta Part B: At. Spectrosc. 175.

Lehmann, P.H., Chmelickova, H., Osten, W., Sebestova, H., Havelkova, M., Albertazzi, A., Rihakova, L., Nozka, L., 2013. Laser welding control by monitoring of plasma. Opt. Meas. Syst. Ind. Insp. VIII.

Li, J., Zhang, Y., Liu, W., Li, B., Yin, X., Chen, C., 2022. Prediction of penetration based on plasma plume and spectrum characteristics in laser welding. J. Manuf. Process. 75, 593–604.

Naeem, M., Montello, A., 2022, Laser Welding of Dissimilar Materials for Electric Vehicle Batteries, Proceedings of the 38th International MATADOR Conference, pp. 751–761.

Nilsen, M., Sikström, F., Christiansson, A.-K., Ancona, A., 2017. Vision and spectroscopic sensing for joint tracing in narrow gap laser butt welding. Opt. Laser Technol. 96, 107–116.

Oezmert, A., Drenker, A., Nazery, V., 2013. Detectability of penetration based on weld pool geometry and process emission spectrum in laser welding of copper. Phys. Procedia 41, 509–514.

Sadeghian, A., Iqbal, N., 2022. A review on dissimilar laser welding of steel-copper, steel-aluminum, aluminum-copper, and steel-nickel for electric vehicle battery manufacturing. Opt. Laser Technol. 146.

Schmalen, P., Plapper, P., Asme, 2018, Spectroscopic Studies of Dissimilar Al-Cu Laser Welding, 13th ASME International Manufacturing Science and Engineering Conference, Coll Stn, TX.

Sibillano, T., Ancona, A., Rizzi, D., Rodil, S.S., Nieto, J.R., Konuk, A.R., Aarts, R., Huis in't Veld, A.J., 2010. Study on the correlation between plasma electron temperature and penetration depth in laser welding processes. Phys. Procedia 5, 429–436.

Sibillano, T., Rizzi, D., Ancona, A., Saludes-Rodil, S., Rodríguez Nieto, J., Chmelíčková, H., Šebestová, H., 2012a. Spectroscopic monitoring of penetration depth in CO_2 Nd:YAG and fiber laser welding processes. J. Mater. Process. Technol. 212, 910–916.

Sibillano, T., Rizzi, D., Mezzapesa, F.P., Lugara, P.M., Konuk, A.R., Aarts, R., In 't Veld, B. H., Ancona, A., 2012b. Closed Loop Control of Penetration Depth during CO_2 Laser Lap Welding Processes. Sensors 12, 11077–11090.

Solchenbach, T., Plapper, P., Cai, W., 2014. Electrical performance of laser braze-welded aluminum–copper interconnects. J. Manuf. Process. 16, 183–189.

Song, M., Wu, L., Liu, J., Hu, Y., 2021. Effects of laser cladding on crack resistance improvement for aluminum alloy used in aircraft skin. Opt. Laser Technol. 133.

Stavridis, J., Papacharalampopoulos, A., Stavropoulos, P., 2017. Quality assessment in laser welding: a critical review. Int. J. Adv. Manuf. Technol. 94, 1825–1847.

Wang, Z., Shen, J., Hu, S., Wang, T., Bu, X., 2020. Investigation of welding crack in laser welding-brazing welded TC4/6061 and TC4/2024 dissimilar butt joints. J. Manuf. Process. 60, 54–60.

Wu, Y., Guo, L., Xiao, L., Sun, S., 2021. Influence of Laser Welding Parameters on Weld Formation and Mechanical Properties of Cu/Al Dissimilar Materials. Hot Working. Technology 50, 17.

Yang, T.Y.B., Kruer, W.L., More, R.M., Langdon, A.B., 1995. Absorption of laser light in overdense plasmas by sheath inverse bremsstrahlung. Phys. Plasmas 2, 3146–3154.

Yu, J., Lee, H., Kim, D.-Y., Kang, M., Hwang, I., 2020. Quality assessment method based on a spectrometer in laser beam welding process. Metals 10.

Yusof, M.F.M., Ishak, M., Ghazali, M.F., 2017. Feasibility of using acoustic method in monitoring the penetration status during the Pulse Mode Laser Welding process. Iop Conf. Ser. -Mat. Sci. 238.

Yusof, M.F.M., Ishak, M., Ghazali, M.F., 2020. Classification of weld penetration condition through synchrosqueezed-wavelet analysis of sound signal acquired from pulse mode laser welding process. J. Mater. Process. Technol. 279.

Zhang, Y., Li, F., Liang, Z., Ying, Y., Lin, Q., Wei, H., 2018. Correlation analysis of penetration based on keyhole and plasma plume in laser welding. J. Mater. Process. Technol. 256, 1–12.

Zhang, Y., You, D., Gao, X., Katayama, S., 2019. Online monitoring of welding status based on a DBN model during laser welding. Engineering 5, 671–678.

Zhang, Z., Li, B., Zhang, W., Lu, R., Wada, S., Zhang, Y., 2020. Real-time penetration state monitoring using convolutional neural network for laser welding of tailor rolled blanks. J. Manuf. Syst. 54, 348–360.